Tungsten fiber-reinforced tungsten composites and their thermal stability

Wartacz, Daniel Ahlin Heikkinen; Riesch, Johann; Pantleon, Karen; Pantleon, Wolfgang

Published in:
Journal of Nuclear Materials

Link to article, DOI:
10.1016/j.jnucmat.2024.154951

Publication date:
2024

Document Version
Publisher's PDF, also known as Version of record

Journal of Nuclear Materials 592 (2024) 154951

Contents lists available at ScienceDirect

Journal of Nuclear Materials

journal homepage: www.elsevier.com/locate/jnucmat

Tungsten fiber-reinforced tungsten composites and their thermal stability

Daniel Ahlin Heikkinen Wartacz [a,*], Johann Riesch [b], Karen Pantleon [a], Wolfgang Pantleon [a]

[a] Department of Civil and Mechanical Engineering, Technical University of Denmark, Produktionstorvet 425, Kongens Lyngby, 2800, Denmark
[b] Max Planck Institute for Plasma Physics, Boltzmannstraße 2, Garching, 85748, Germany

ARTICLE INFO

Keywords:
Thermal stability
Tungsten
Tungsten fiber-reinforced tungsten composite
Recrystallization
Grain growth

ABSTRACT

Tungsten will be used as armor material for plasma-facing components in future fusion reactors, but its propensity to embrittlement by microstructural restoration at high temperatures poses a challenge for its use. Tungsten fiber-reinforced tungsten composites (W_f/W) with drawn tungsten wires embedded in a polycrystalline tungsten matrix remedy the inherent brittleness of tungsten and achieve pseudo-ductile behavior via extrinsic toughening mechanisms. As plasma-facing materials experience high heat fluxes during operation, their thermal stability is important. In W_f/W composites, the restoration processes at high temperatures differ significantly between wires and matrix: initially recrystallization dominates in the wires, as they were plastically deformed during wire drawing, whereas abnormal grain growth occurs in the matrix. Growing grains may obstruct the interface between wire and matrix and deteriorate the otherwise improved fracture properties of W_f/W. An yttria interlayer is introduced to separate wire from matrix, to hinder an interplay between the restoration processes and to impede grains from the wire from growing into the matrix and vice versa. Cylindrical model systems containing a single wire in a chemically vapor-deposited matrix are investigated without any interlayer and with an yttria interlayer of either 1 μm or 3 μm thickness. Isothermal annealing at 1450 °C for different times up to 2 weeks, followed by microstructural characterization by means of EBSD are carried out to characterize the microstructural evolution. The role of the interlayer on the microstructural evolution is elucidated to establish if decoupling of the restoration processes is actually achieved.

1. Introduction

Tungsten and tungsten-based materials are chosen as plasma-facing armor materials, because tungsten has the highest melting point of all metals, exhibits good thermal conductivity and has good strength and creep resistance at elevated temperatures [1]. These qualities are essential for materials used in plasma-facing components of future fusion reactors [2]. The intrinsic brittle behavior at room temperature of undeformed bulk tungsten with body-centered cubic crystal structure can be overcome by plastic deformation to high strains [3,4]. Tungsten fiber-reinforced tungsten composites (W_f/W) consisting of drawn tungsten fibers (ductile at room temperature [3]) in a brittle tungsten matrix exhibit pseudo-ductile behavior at room temperature by activating extrinsic toughening mechanisms during deformation [5–7]. The pseudo-ductile behavior stems from (i) the ductility of the fibers, obtained by the deformation microstructure when drawn during manufacturing, and (ii) their ability to debond and getting pulled out of the matrix during deformation [7]. Currently, there are two routes for producing W_f/W, by chemical vapor deposition (CVD) [8] or through powder metallurgy [9].

W_f/W composites have not yet been qualified as plasma-facing material in terms of thermal stability, given the high heat loads experienced during operation. Exposure of W_f/W composites to high temperatures causes abnormal grain growth in the matrix in the vicinity of the fiber, while recrystallization occurs in the fiber [10]. If these restoration processes interconnect the microstructures of matrix and fiber, the otherwise improved mechanical properties will be lost. Separation of the two evolving microstructures is detrimental to sustain the improved mechanical properties of W_f/W. Attempting to enhance their thermal stability, an interlayer between the fibers and the matrix is introduced. This interlayer shall serve as a barrier to separate the microstructure evolution of fiber and matrix.

To assess the thermal stability of W_f/W composites and a potential breakdown of the interface, high temperature annealing at 1450 °C for different durations is conducted. The resulting microstructural evolution is characterized by means of electron backscatter diffraction

* Corresponding author.
E-mail address: dahwa@dtu.dk (D.A.H. Wartacz).

https://doi.org/10.1016/j.jnucmat.2024.154951
Received 10 November 2023; Received in revised form 22 January 2024; Accepted 3 February 2024
Available online 13 February 2024

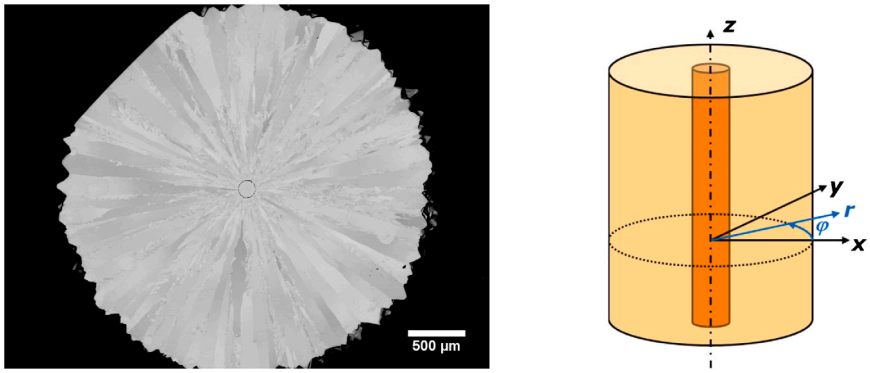

Fig. 1. Single fiber W_f/W model composites: a) Secondary electron image displaying a cross section of a W_f/W composite with a 3 µm thick Y_2O_3 interlayer (seen as a black ring in the center) in the as-processed state (with a ground chamfer at the upper left corner to distinguish different composites). b) Schematic representation featuring the coordinate systems used. The dashed line indicates a cross section of the rod.

(EBSD). The materials studied in this investigation are cylindrical model systems produced by depositing a tungsten matrix onto a single tungsten wire serving as fiber, using CVD [11]. Model W_f/W composites with and without an yttria interlayer between fiber and matrix are investigated.

2. Material and methods

2.1. Material

Three different W_f/W model systems are produced [12]: without an interlayer or with either a 1 µm or a 3 µm thick yttria interlayer. Drawn tungsten wires, commercially produced by OSRAM GmbH with a diameter of 150 µm and doped with 60 ppm of potassium, are used as fibers. The yttria interlayers are deposited onto the fibers by physical vapor deposition (magnetron sputtering) before the matrix is chemically vapor-deposited (cf. [11]). After the CVD process, rods with diameters between 2.7 mm and 3.5 mm are obtained and cut to a length of about 40 mm. A cross-sectional view and a visual representation of the single fiber composite are shown in Fig. 1.

2.2. Experimental procedure

The obtained rods are cut into discs with an Accutom-50 from Struers of either 0.5 mm or 1.3 mm thickness. Before cutting, the rods are hot-embedded at 150 °C for 7 min to give extra support; after cutting, the embedding resin is removed again. Annealing at the high temperature of 1450 °C is carried out in a tube furnace NaberTherm RHTH 50-150/18. Previous to annealing, three disc-shaped specimens with different interlayers (distinguishable by chamfers) are encapsulated together in a quartz glass ampule. To ensure a non-oxidizing environment in the ampules, they are evacuated, flushed with argon, and evacuated again before sealing. The furnace is pre-heated before the ampules are placed inside. After annealing for the desired time up to 2 weeks, the ampules with the three specimens inside are removed from the furnace and opened after air-cooling to room temperature. Different specimens are used for each annealing time.

To investigate the microstructure of the samples, one of the surfaces of each disc-shaped specimen is ground with SiC paper up to 4000 grit size, polished with a 3 µm diamond suspension and electropolished for approximately 7 s in a 3% NaOH solution. Electropolishing is performed with a voltage of 12 V and a current of 2 A. Orientation data are collected on the prepared surface (corresponding to a cross section of the cylindrical model system) using either a Zeiss Sigma SEM equipped with a Cnano EBSD detector from Oxford instruments or a Zeiss Supra SEM using a Oxford Instruments Nordlys3 EBSD detector. Square grids with different step sizes (1 µm or 5 µm) are used depending on the size of the area to be analyzed and the purpose of acquisition; the accelerating voltage is 20 kV. All orientation maps are presented and analyzed without any filtering or removal of non-indexed points. In the orientation maps, high angle boundaries (HABs) are considered to be present between neighboring points for disorientation angles above 15° and indicated black; low angle boundaries (LABs) for disorientation angles above 2°, but less than 15° are indicated in white. The evaluation of the EBSD data is done with the Matlab plugin toolbox MTEX Version 5.8.1 [13] and evaluated further by purposely derived routines (see subsections 3.1 and 3.5).

3. Results

3.1. As-processed state — W_f/W with a 3 µm thick yttria interlayer

Orientation maps of a cross section of the single fiber composite with 3 µm thick interlayer in its as-processed state are presented in Fig. 2 (the as-processed states of the two other W_f/W composites have been discussed earlier [12]). In the overview orientation map in Fig. 2a mainly the matrix can be observed where wedge-shaped grains have grown radially outwards during the CVD process. In the close orientation map in Fig. 2b more details are discerned. Only parts of the large wedge-shaped grains are seen as well as a corona of small needle-like grains in the CVD matrix in the vicinity of the interlayer. The interlayer itself can be identified by a ring of non-indexed points (in white). The deformation structure within the wire is characterized by (elongated) grains with tiny cross sections [10]. The greenish color reveals an alignment of one of the ⟨110⟩ direction with wire axis (z-axis) as expected from the wire drawing process resulting in a ⟨110⟩ fiber texture [14].

The colors representing the crystallographic directions along the z-axis in the matrix appear similar to the colors of the matrix of a single fiber composite with 1 µm thick yttria interlayer in its as-processed state as presented in [12]. In accordance with [15], a cylindrical coordinate system is employed in order to unambiguously characterize the crystallographic texture. For each pixel the Euler angle φ_1 (not φ_2 as is erroneously mentioned in [15]) is adjusted by the azimuthal angle φ of the pixel. In this manner, the crystallographic directions aligned with the radial direction pointing radially outwards from the center of the wire are highlighted in Fig. 3. The dominating red color reveals that ⟨100⟩ directions preferably align with the radial direction indicating the existence of a cyclic ⟨100⟩ ring fiber texture (cf. [16]) known to be prevalent in the CVD matrix of single fiber W_f/W composites [12,15]. The two pole figures with respect to the cylindrical coordinate system in Fig. 3b confirm the cyclic ⟨100⟩ ring fiber texture by the pole density in the 100 pole figure being highest along the radial direction and the rotational symmetry around this direction, which is further supported by the 110 pole figure. The volume fraction of all orientations

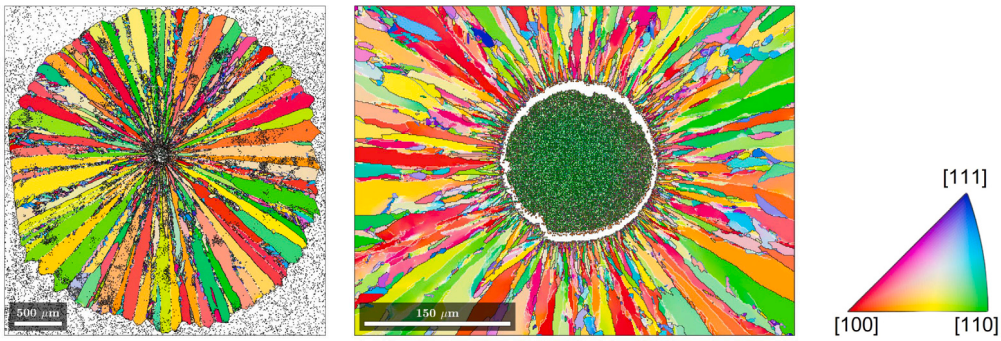

Fig. 2. Orientation maps of the cross section of a single tungsten fiber-reinforced tungsten composite with a 3 µm thick yttria interlayer in the as-processed state: (a) overview map acquired with a step size of 5 µm, (b) close map acquired with a step size of 1 µm. The colors reflect the crystallographic directions along the axial direction according to the inverse pole figure. (For interpretation of the colors in the figure(s), the reader is referred to the web version of this article.)

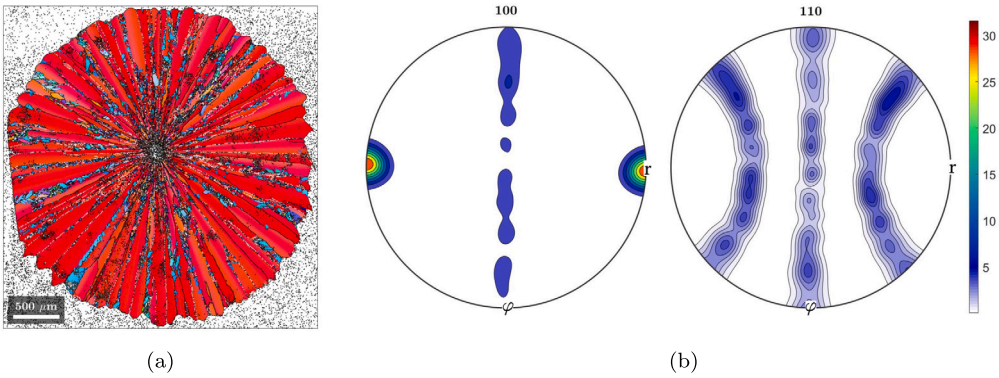

Fig. 3. (a) Orientation map of the cross section of a single tungsten fiber-reinforced tungsten composite with a 3 µm thick yttria interlayer in the as-processed state. The colors reflect the crystallographic directions along the radial direction according to the inverse pole figure of Fig. 2. (b) Corresponding 100 and 110 pole figures. All pole densities are presented with respect to a cylindrical coordinate system in stereographic projection.

with ⟨100⟩||r is 86% when allowing maximal 15° deviation between the radial direction and the closest ⟨100⟩ direction. A second texture component, a cyclic ⟨221⟩ ring fiber texture (⟨221⟩||r), constituting another 10% of the volume, is caused by twinning (as ⟨221⟩ is the twinning direction of ⟨100⟩ [17,18]).

3.2. Annealed states — W_f/W without interlayer

In Fig. 4a orientation maps depicting different annealing states are shown for a W_f/W single fiber composite without any interlayer. Consequently, fiber and matrix have a common interface. To allow comparison between orientation maps of different magnifications, the scale bar represents the original wire diameter of 150 µm in all close orientation maps.

Comparing the microstructure after annealing at 1450 °C for 1 day in Fig. 4b with the one of the as-processed state in Fig. 4a reveals little changes in the fiber itself. Some marginally larger grains appear in the fiber indicating initiation of recrystallization in the deformation structure (subtle changes due to recovery cannot be recognized on the used magnification). The small needle-like matrix grains in the vicinity of the fiber have grown slightly as visible when comparing to the as-processed state. The microstructure of the matrix with wedge-shaped grains and a preferred ⟨110⟩ direction along the wire axis as observed in the as-processed state (cf. Fig. 4a and [12]) is still present after annealing at 1450 °C for 1 day in Fig. 4b. The interface between matrix and fiber is hard to discern due to the absence of any interlayer and the pronounced ⟨110⟩ fiber texture of the drawn wire having a preferred ⟨110⟩ direction along the wire axis as well [12]. The overall impression of the microstructure after 2 days of annealing at 1450 °C, displayed in Fig. 4c, is similar to that after 1 day of annealing. There are no significant changes in the fiber itself and the small grains just outside the fiber grew moderately in size.

The microstructure changed entirely after 1 week of annealing at 1450 °C. In Fig. 5d neither the fiber, nor its deformation structure is discernible any longer. Huge grains have replaced the local microstructure in the fiber and its surroundings (not only in its vicinity). The region that previously contained the wire is now composed of only a few large grains. As evident from their different colors, these grains do not have one of their ⟨110⟩ directions aligned with the wire axis. Presumably, these grains with new orientations formed during recrystallization of the fiber and grew tremendously afterwards.

3.3. Annealed states — W_f/W with a 1 µm thick yttria interlayer

The microstructure evolution of the W_f/W composite with 1 µm thick interlayer of yttria behaves quite similar to that of the composite without interlayer as seen from the orientation maps of various annealing states in Fig. 5. The scale bar represents again the original diameter of the drawn wire of 150 µm to allow proper comparison.

As depicted in Fig. 5b, the fiber still maintains its (recovered) deformation structure after 1 day of annealing at 1450 °C. Subtle changes have occurred just outside the fiber. The fine, needle-shaped grains have grown in comparison to the as-processed state (Fig. 5a). Similar phenomena are observed in the microstructure after 2 days of annealing in Fig. 5c: no significant changes in the fiber, but the fine, needle-like grains in its vicinity grew bigger in size.

The yttria interlayer can still be recognized by the presence of a (white) ring of non-indexed pixels after annealing at 1450 °C up to 2

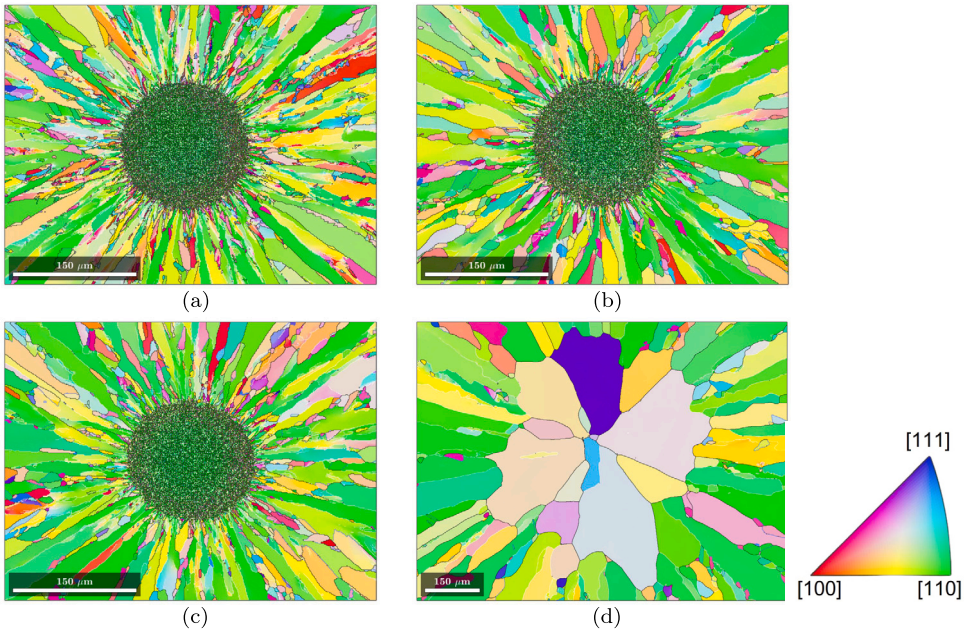

Fig. 4. Orientation maps of cross sections from as-processed and annealed single tungsten fiber-reinforced tungsten composites without any interlayer: (a) As-processed or annealed at 1450 °C for different times (b) 1 day, (c) 2 days, and (d) 1 week. The colors reflect the crystallographic directions along the axial direction according to the inverse pole figure. All scale bars represent the original diameter of 150 μm of the drawn wire.

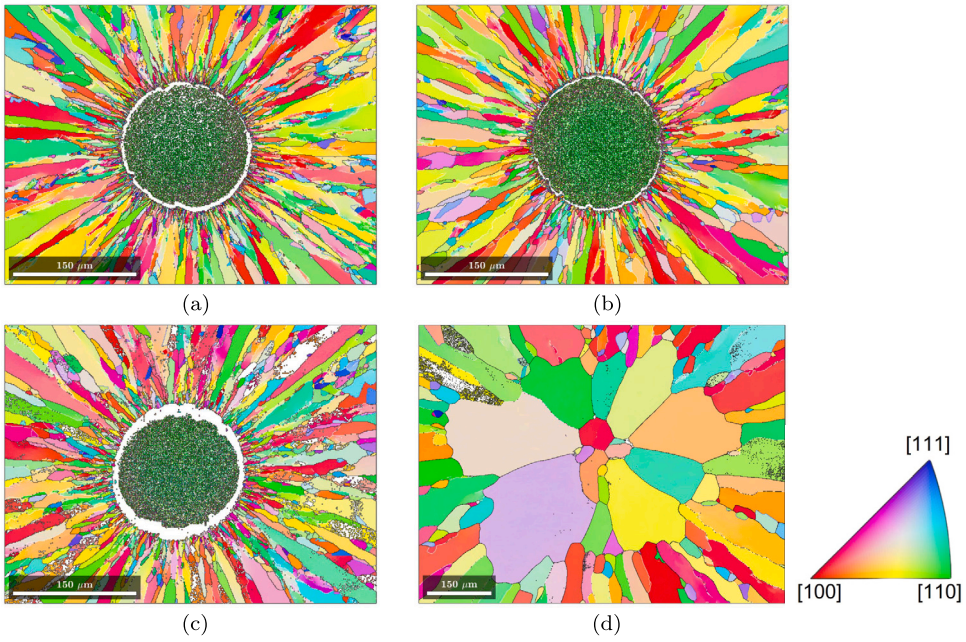

Fig. 5. Orientation maps of cross sections from as-processed and annealed single tungsten fiber-reinforced tungsten composites with a 1 μm thick yttria interlayer: (a) As-processed or annealed at 1450 °C for different times (b) 1 day, (c) 2 days, and (d) 1 week. The colors reflect the crystallographic directions along the axial direction according to the inverse pole figure. All scale bars represent the original diameter of 150 μm of the drawn wire.

days. The difference between its appearance in the different maps is attributed to different acquisition conditions and presumably slight differences in electropolishing (as the yttria interlayer is less affected than tungsten by the solution used).

After annealing at 1450 °C for 1 week, neither the wire, nor the interlayer are distinguishable any longer as presented in Fig. 5d. The grains within the wire have new orientations not belonging to the ⟨110⟩ fiber texture. They have undergone recrystallization followed by substantial grain growth. In the center of the map, where the fiber should be located, only a few grains are present and surrounded by even larger ones. No trace of the deformation structure of the wire is found any longer. Its original position is perceptible only by the sole remnants of the interlayer appearing as white non-indexed pixels located close to the center.

3.4. Annealed states — W_f/W with a 3 μm thick yttria interlayer

The microstructural changes in the W_f/W composite with 3 μm thick yttria interlayer follow the pattern of the two other composites. In Fig. 6, orientation maps are presented of W_f/W with an yttria interlayer of 3 μm thickness after five different times of annealing at 1450 °C;

two additional annealing times, 4 days and 2 weeks, are provided to reveal the restoration kinetics (cf. section 3.5). As before, the scale bars in the maps represent the original diameter of the wire, 150 μm, in order to allow proper comparison between the different states of the samples represented in the orientation maps.

As for the composites without an interlayer or a 1 μm thick yttria interlayer, the microstructure after 1 day of annealing shown in Fig. 6a remains similar to the as-processed state (shown in Fig. 2b). The alignment of ⟨110⟩ directions with the wire axis is still present in the fiber; the small needle-like grains just outside of the fiber seem to have grown slightly. The same impression is given by the orientation map in Fig. 6b displaying the microstructure after 2 days of annealing, where the grains just outside of the fiber also have grown in size.

After 4 days of annealing at 1450 °C, the yttria interlayer can still be discerned in the orientation map in Fig. 6c, but the interlayer is not fully intact any longer and changes in its geometry are obvious. At several locations along the perimeter of the wire, grains from the matrix now border grains within the fiber. Nevertheless, the interface between both is mostly preserved and no grains have crossed over between fiber and matrix. It appears as though fiber and matrix are still separated. Further microstructural changes can be observed in the orientation map both within the fiber and its vicinity. In the fiber, large grains have replaced its deformation structure. Their orientations are different from that of the as-processed state (where the green color e.g. in Fig. 2b shows an alignment of the ⟨110⟩ directions with the z-axis) as seen by the many different colors, not observed prior to annealing. Just outside the fiber, the small needle-like grains found in the as-processed state have grown considerably large.

After annealing at 1450 °C for 1 week, the original position of the wire cannot unambiguously be identified in the microstructure in Fig. 6d. The center of the map consists of only a few grains surrounded by huge grains in the matrix. The yttria interlayer is almost unrecognizable and only small islands of yttria (regions of non-indexed points in white) are seen in the center of the orientation map as remaining trace of the interlayer. The entire affected area appears significantly larger than after 4 days of annealing.

Finally, after 2 weeks of annealing at 1450 °C, the fiber is no longer distinguishable in Fig. 6e and small traces of yttria can hardly give an indication. Instead, the region comprising the location, where the fiber has been originally and its surroundings, consists of only 12 huge grains as the grains in the affected region grew tremendously after initial recrystallization in the fiber.

3.5. Size determination from orientation data

In an attempt to elucidate the restoration kinetics, the affected region around the fibers replacing the deformation structure of the wire and its surrounding is identified and its size is quantified as well as that of the grains constituting it.

As initial step, grains are assembled in an orientation map as contiguous regions of pixels with close orientations separated by boundaries with disorientation angles of at least 2°. Grains to be considered must consist of at least 10 valid pixels (non-indexed points associated with a grain by MTEX are ignored and removed from the individual grain).

An area affected by enormous grain growth in the sample annealed at 1450 °C for 4 days or longer is observed consistently close the original position of the fiber. This area contains huge grains significantly larger than the grains in the deformation structure of the fiber in its as-processed state and matrix grains in the vicinity of the fiber. In order to quantify these affected areas and different sizes within, the following procedure is adapted and illustrated in Fig. 7:

1. Resolving the affected area: For an initial approximation of the affected area, a circle is inscribed manually in the observed region of huge grains containing most of the affected area. The circle is chosen to be completely within the affected area as demonstrated by the blue circle in Fig. 7a.
2. Properly defining the affected area: To determine whether a grain belongs to the affected area, its center of mass is found. If the center of mass of a grain lies inside the inscribed circle, that grain is considered to belong to the affected area. Grains are excluded, if their center of mass lies outside of the circle. Based on the circle depicted blue in Fig. 7a, the grains belonging to the affected area and the affected area itself are identified as shown in Fig. 7b.
3. Size determination: The sizes of the grains and that of the entire affected area (as combination of all pixels belonging to grains forming it) are reported as equivalent circular diameters (ECD) $D = \sqrt{4A/\pi}$. The areas $A = N\Delta x^2$ are determined from the number N of pixels belonging to the entity and the step size Δx. If regions belonging to the fiber remain unrecrystallized or still show small grains after annealing, these regions are excluded from the determination of the mean grain size but included in the size determination of the affected area.

Affected areas are successfully identified and quantified for all annealing treatments at 1450 °C lasting at least for 4 days (i.e. for which huge grains were observed). The results for the W_f/W composite with a 3 μm thick yttria interlayer are combined in Fig. 8. After 4 days of annealing an area with an ECD of 294 μm is affected by large grains of an average ECD of 24 μm, the largest grain having an ECD of 83 μm. With annealing progress all three quantities increase strongly. Already after 1 week at 1450 °C, the affected area has grown by a factor of 7 (its ECD by a factor of 2.6), the average ECD of the grains by a factor of 4.8 similar to the ECD of the largest grain. After 1 week of annealing the composite with a 3 μm interlayer has the biggest affected area with an ECD of 774 μm, the largest mean grain size within the affected area and the largest individual grain in this area, compared to the composite with no interlayer and the composite with 1 μm interlayer for which the affected areas have an ECD of 578 μm and 546 μm respectively. All affected areas are much larger than the cross section of the initial tungsten wire.

4. Discussion

The microstructural investigations after annealing presented here (in combination with the observations in [12] on the same model systems) allow to deduce a comprehensive picture of the restoration processes occurring at 1450 °C in single tungsten fiber-reinforced tungsten model composites even independent of the presence of an yttria interlayer.

During the first 2 days of annealing at 1450 °C, only minor changes occur. In the matrix, the size of the fine needle-shaped grains in the vicinity of the fiber increases slightly by grain growth, while changes are hardly recognized in the fiber. Taking into account the high temperature of annealing, it is expected that the deformation structure recovers and recrystallization initiates as indicated by a few marginally larger grains. To track the progress of recovery and recrystallization within the drawn wire either acquisition of orientation maps with even higher resolution or performing micro hardness testing (similar to the approach in [19]) could be considered.

After 4 days of annealing at 1450 °C, the microstructure is altered substantially. The deformation structure of the drawn wire is replaced by a few large grains with orientations not belonging to the ⟨110⟩ fiber texture from wire drawing. Recrystallization followed by grain growth has occurred. This is particularly obvious for the W_f/W composites without an interlayer and with a 1 μm thick yttria interlayer where the large grains after annealing for 4 days are still confined to the region of the wire (see Figs. 7b and 8b in [12], respectively). For the W_f/W composite with a 3 μm thick yttria interlayer, the recrystallized grains in the wire and the abnormally grown grains in its vicinity are of almost equal size after 4 days of annealing at 1450 °C. The origin of the grains in the wire from recrystallization of its deformation structure

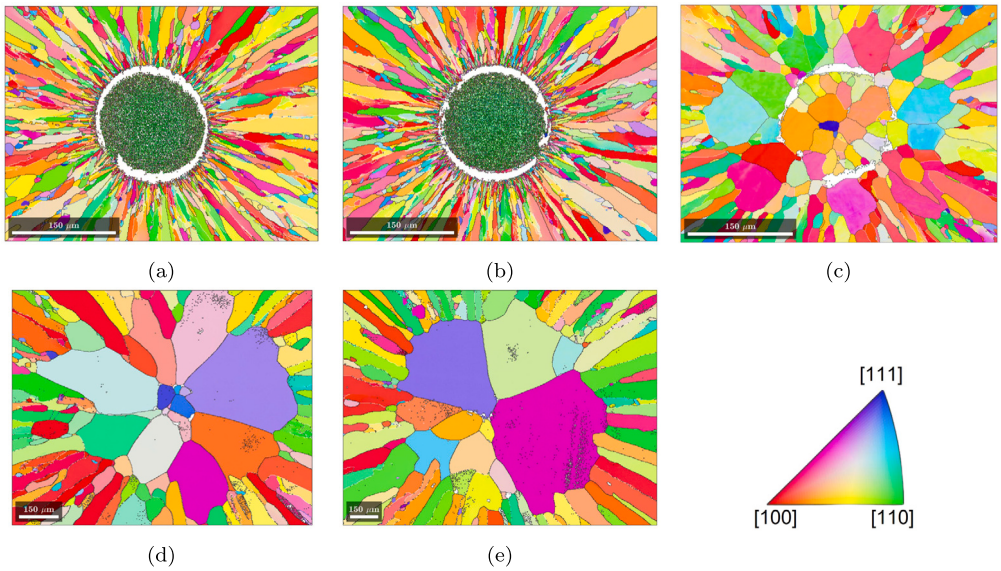

Fig. 6. Orientation maps of cross sections from single tungsten fiber-reinforced tungsten composites with a 3 μm thick yttria interlayer after annealing at 1450 °C for different times: (a) 1 day, (b) 2 days, (c) 4 days, (d) 1 week and (e) 2 weeks. The colors reflect the crystallographic directions along the axial direction according to the inverse pole figure. All scale bars represent the original diameter of 150 μm of the drawn wire.

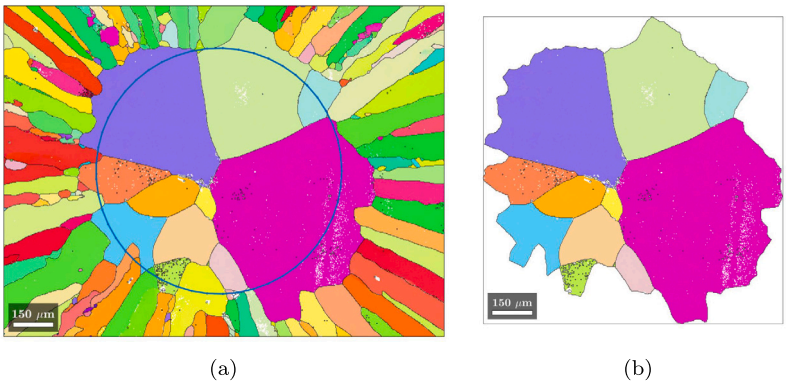

Fig. 7. Orientation maps of the cross section of a single tungsten fiber-reinforced tungsten composite with a 3 μm thick yttria interlayer after annealing at 1450 °C for 2 weeks. (a) Close map with a blue circle to preliminary define the affected area to be quantified. (b) Properly defined affected area as combination of all grains with center of mass within the inscribed circle.

is nevertheless obvious from the remainders of the yttria interlayer in Fig. 6c.

While the yttria interlayer remains intact for the first two days of annealing at 1450 °C, it is not continuous any longer and deteriorated to some extent after 4 days of annealing. After 1 week and 2 weeks of annealing the yttria interlayer appears fully disintegrated. For both W_f/W composites with an yttria interlayer in their as-processed state, the sole remainder of this interlayer can be traced as only small particles of yttria close to the center. Driven by phase boundary energy and reduction of phase boundary area, yttria appears to have spheroidized into individual spherical particles instead of the original layer constituting a hollow cylinder. In consequence, as the interlayer disintegrates during annealing at 1450 °C, the thermal stability of the W_f/W composites with yttria interlayer is not enhanced compared to the W_f/W composite without an interlayer. During annealing at 1450 °C for 1 week or 2 weeks, abnormal grain growth causes formation of huge grains consuming the wire as well as its surrounding. Quantitative analysis reveals that after 1 week of annealing at 1450 °C, the W_f/W composite with 3 μm interlayer exhibits the largest grain sizes as well as the largest affected area. The precise explanation for this observation remains elusive, and further investigations are needed to uncover the underlying reasons.

The microstructure developing at 1450 °C after 1 or 2 weeks are strikingly different from previous observations of restoration of similar W_f/W model composites with and without oxide interlayers [10], where even after annealing for 4 weeks at 1400 °C no such large affected areas with huge grains were observed. Additionally, the oxide interlayer spheroidized to some extent, but did not disintegrate entirely. The modest increase in annealing temperature of 50 K seem to exert a significant impact on the composites, evident in the recrystallization of the fiber and the breakdown of the yttria interlayer. These phenomena ultimately lead to abnormal grain growth, resulting in huge grains occupying the location originally occupied by the fiber. Presuming a single thermally activated restoration process with a reaction rate $\dot{\Gamma} = \nu \exp(-Q/RT)$ following an Arrhenius behavior (with a jump frequency ν, the universal gas constant R, the absolute temperature T, cf. [20]) and an activation energy Q of 579 kJ/mol typical for recrystallization processes in deformed tungsten [20,21], the temperature increase by 50 K from 1400 °C to 1450 °C should cause an increase in the restoration rate by a factor of 3.3. The progress of a thermal activated process after 4 weeks at 1400 °C should be equivalent to that after 1.2 weeks at 1450 °C. Consequently, one would expected to have seen similar phenomena as observed here for the longest annealing time of 4 weeks at the lower temperature of 1400 °C in the earlier study [10]. Longer an-

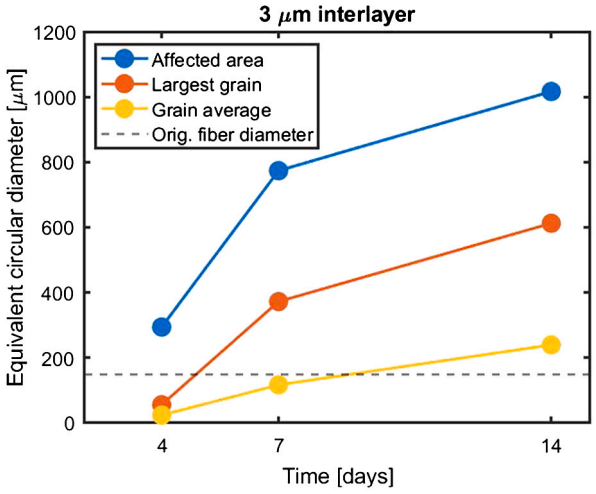

Fig. 8. Quantification of area affected by substantial grain growth of a single tungsten fiber-reinforced tungsten composite with a 3 μm thick yttria interlayer after annealing at 1450 °C from 4 days to 2 weeks: ECD of the entire affected area, ECD of the largest grain and the average ECD of all grains in the affected area. The dashed line represents the original diameter of 150 μm of the drawn wire.

nealing treatments of the present W_f/W model composites at 1400 °C will settle, if the phenomenon was previously just missed at the lower temperature, if a higher activation energy Q is governing the process or if the slightly different manufacturing conditions of the W_f/W model composites from different batches caused the discrepancy.

It must be mentioned, that the yttria interlayers are physically-vapor deposited on the wires by magnetron sputtering in two steps. After deposition of an yttria layer with desired thickness on one side of the wires, the frame is turned by 180° to deposit yttria on the other side. Achieving an interlayer with homogeneous thickness can be challenging in view of the line-of-sight nature of the process. Previous investigations have reported tungsten bridges between fiber and matrix in the yttria interlayers [22]. Such discontinuities in the yttria interlayer can be spotted e.g. for the W_f/W composite with 3 μm interlayer after 1 day of annealing in Fig. 6a as a missing section of the interlayer on the lower left side of the fiber. A corresponding discontinuity can be seen in Fig. 6b after 2 days of annealing on the lower right side. Considering that both samples are cut consecutively from the same rod, both discontinuities most likely represent the same imperfection in the interlayer which has already been present in the as-processed state.

Despite the imperfections in the yttria interlayer in its as-processed state, the interlayer is significant for the mechanical behavior of the W_f/W composites and their performance as plasma-facing material. Even if the drawn tungsten wire recrystallizes fully, the propensity of wire debonding from the CVD matrix will account for some pseudo-ductile behavior. Wire debonding will allow crack deflection along the interface between fiber and matrix, cause energy dissipation and thereby increase the toughness of the composite [23]. In this respect, the apparent lack of thermal stability of the microstructure at 1450 °C becomes crucial as the interlayer disintegrates and tungsten fibers and matrix cannot be distinguished any longer. Therefore, other kinds of interlayers in W_f/W composites and their restoration behavior should be explored, e.g. ZrO [24] or ZrC which has shown beneficial properties in dispersion-strengthened tungsten composites due to coherent interfaces [25].

5. Summary

Tungsten fiber-reinforced tungsten composites with and without an yttria interlayer, either 1 μm or 3 μm, between the fiber and the matrix are investigated. The model system composites used for the investigation, were produced by a CVD process depositing a tungsten matrix on drawn tungsten wires acting as fibers. Electron backscatter diffraction of the model composite with a 3 μm thick yttria interlayer revealed in its as-processed condition a matrix with columnar, wedge-shaped grains and a cyclic ⟨100⟩ ring fiber texture.

The single fiber model composites were annealed at 1450 °C for different periods of time. Up to 2 days of annealing, only minor changes in the microstructures due to restoration were observed for each of the composites. After 4 days of annealing at 1450 °C, the composite with a 3 μm thick yttria interlayer shows severe microstructural alterations. In the fiber, grain growth takes place after recrystallization. Despite substantial grain growth in the fiber and its vicinity, fiber and matrix can still be distinguished. After 1 week of annealing at 1450 °C, the fiber and the matrix adjacent to it are hardly separable from each other, regardless of the presence of an interlayer; the composite with 3 μm thick yttria interlayer has the largest affected area, the largest individual grain and the highest mean grain size in the affected area. After 2 weeks of annealing, the grains and the affected area become even larger.

6. Conclusions

The findings of this investigation suggest that the separation of the fiber and the matrix can neither be withheld without an interlayer, nor with an yttria interlayer for prolonged periods of time at 1450 °C. The thicker yttria interlayer (3 μm compared to 1 μm) is not performing better, rather the opposite. At the investigated temperature, the composites are not sufficiently thermally stable, in particular the interlayer cannot prevent an intergrowth between fiber and matrix. In consequence, that could mean that composites with such yttria interlayers may lose their pseudo-ductility during temporary overheating while operating as plasma-facing material of a divertor and their application should be restricted to lower temperatures.

CRediT authorship contribution statement

Daniel Ahlin Heikkinen Wartacz: Data curation, Formal analysis, Investigation, Methodology, Software, Visualization, Writing – original draft. **Johann Riesch:** Supervision, Writing – review & editing. **Karen Pantleon:** Supervision, Writing – review & editing. **Wolfgang Pantleon:** Conceptualization, Formal analysis, Funding acquisition, Methodology, Software, Supervision, Writing – original draft, Writing – review & editing.

Declaration of competing interest

The authors declare that they have no known competing financial interests or personal relationships that could have appeared to influence the work reported in this paper.

Data availability

Data will be made available on request.

Acknowledgements

This work has been carried out within the framework of the EUROfusion Consortium, funded by the European Union via the Euratom Research and Training Programme (Grant Agreement No 101052200 – EUROfusion). Views and opinions expressed are however those of the authors only and do not necessarily reflect those of the European Union or the European Commission. Neither the European Union nor the European Commission can be held responsible for them. The authors acknowledge the support of Alexander Lau from Forschungszentrum Jülich for performing CVD.

References

[1] E. Lassner, W-D. Schubert, Tungsten, Kluwer Academic, New York, 1999, p. 24.
[2] G. Pintsuk, Compr. Nucl. Mater. 4 (2012) 581.
[3] P. Schade, Int. J. Refract. Met. Hard Mater. 28 (2010) 648.
[4] J. Reiser, J. Hoffmann, U. Jäntsch, M. Klimenkov, S. Bonk, C. Bonnekoh, M. Rieth, A. Hoffmann, T. Mrotzek, Int. J. Refract. Met. Hard Mater. 54 (2016) 351.
[5] J. Riesch, M. Aumann, J.W. Coenen, H. Gietl, G. Holzner, T. Höschen, P. Huber, M. Li, C. Linsmeier, R. Neu, Nucl. Mater. Energy 9 (83) (2016).
[6] H. Gietl, J. Riesch, J.W. Coenen, T. Höschen, C. Linsmeier, R. Neu, Fusion Eng. Des. 124 (2017) 400.
[7] J. Riesch, J.Y. Buffiere, T. Höschen, M. Scheel, C. Linsmeier, J.H. You, Nucl. Mater. Energy 15 (2018) 12.
[8] J. Riesch, Y. Han, J. Almanstötter, J.W. Coenen, T. Höschen, B. Jasper, P. Zhao, C. Linsmeier, R. Neu, Phys. Scr. T 167 (2016) 014006.
[9] Y. Mao, J.W. Coenen, J. Riesch, S. Sistla, J. Almanstötter, J. Reiser, A. Terra, C. Chen, Y. Wu, L. Raumann, T. Höschen, H. Gietl, R. Neu, C. Linsmeier, C. Broeckmann, Nucl. Fusion 59 (2019) 086034.
[10] U.M. Ciucani, L. Haus, H. Gietl, J. Riesch, W. Pantleon, J. Nucl. Mater. 543 (2021) 152579.
[11] H. Gietl, J. Riesch, M. Zielinski, T. Höschen, J.W. Coenen, S. Schönen, R. Neu, Nucl. Mater. Energy 28 (2021) 101060.
[12] D.A.H. Wartacz, J. Riesch, K. Pantleon, W. Pantleon, IOP J. Phys. Conf. Ser. 2635 (2023) 012034.
[13] F. Bachmann, R. Hielscher, H. Schaeben, Solid State Phenom. 160 (2011) 63.
[14] W.F. Hosford Jr, Trans. Metall. Soc. AIME 230 (1964) 12.
[15] U.M. Ciucani, L. Haus, H. Gietl, J. Riesch, W. Pantleon, IOP Conf. Ser., Mater. Sci. Eng. 1121 (2021) 012024.
[16] G. Wassermann, J. Grewen, Texturen metallischer Werkstoffe, 2d ed., Springer Verlag, Berlin, 1962, p. 7.
[17] D. Abou-Ras, K. Pantleon, Phys. Stat. Sol. (RRL) 1 (2007) 187.
[18] K. Pantleon, J.A.D. Jensen, M.A.J. Somers, J. Electrochem. Soc. 151 (2008) 45.
[19] U.M. Ciucani, A. Thum, C. Devos, W. Pantleon, Nucl. Mater. Energy 20 (2019) 100701.
[20] W. Pantleon, Phys. Scr. 96 (2021) 124036.
[21] A. Alfonso, D. Juul Jensen, G-N. Luo, W. Pantleon, J. Nucl. Mater. 455 (2014) 591.
[22] H. Gietl, J. Riesch, M. Zielinski, T. Höschen, J.W. Coenen, S. Schönen, R. Neu, Nucl. Mater. Energy 28 (2021) 101060.
[23] J. Du, T. Höschen, M. Rasinski, J-H. You, J. Nucl. Mater. 417 (2011) 472.
[24] J. Du, T. Höschen, M. Rasinski, S. Wurster, W. Grosinger, J-H. You, Compos. Sci. Technol. 70 (2010) 1482.
[25] Z.M. Xie, R. Liu, S. Miao, X.D. Yang, T. Zhang, X.P. Wang, Q.F. Fang, C.S. Liu, G.N. Luo, Y.Y. Lian, X. Liu, Sci. Rep. 5 (2015) 16014.